Inorganic Chemistry

Article

pubs.acs.org/IC

Theoretical Study of Structural, Spectroscopic and Reaction Properties of *trans-bis*(imido) Uranium(VI) Complexes

Yuan-Ru Guo,[‡] Qian Wu,[†] Samuel O. Odoh,[§,∥] Georg Schreckenbach,[§] and Qing-Jiang Pan*[,†]

[†]Key Laboratory of Functional Inorganic Material Chemistry of Education Ministry, School of Chemistry and Materials Science, Heilongjiang University, Harbin 150080, China

[‡]Key Laboratory of Bio-based Material Science & Technology of Education Ministry, College of Material Science and Engineering, Northeast Forestry University, Harbin 150040, China

[§]Department of Chemistry, University of Manitoba, Winnipeg, MB, Canada R3T 2N2

[∥]Environmental Molecular Sciences Laboratory, Pacific Northwest National Laboratory, P.O. Box 999, Richland, Washington 99352, United States

Supporting Information

ABSTRACT: To advance the understanding of the chemical behavior of actinides, a series of *trans-bis*(imido) uranium(VI) complexes, $U(NR)_2(THF)_2(cis\text{-}I_2)$ (**2R**; R = H, Me, ^{t}Bu, Cy, and Ph), $U(NR)_2(THF)_3(trans\text{-}I_2)$ (**3R**; R = H, Me, ^{t}Bu, Cy, and Ph) and $U(N^tBu)_2(THF)_3(cis\text{-}I_2)$ (**3^{t}Bu′**), were investigated using relativistic density functional theory. The axial U═N bonds in these complexes have partial triple bonding character. The calculated bond lengths, bond orders, and stretching vibrational frequencies reveal that the U═N bonds of the *bis*-imido complexes can be tuned by the variation of their axial substituents. This has been evidenced by the analysis of electronic structures. **2H**, for instance, was calculated to show iodine-based high-lying occupied orbitals and U(*f*)-type low-lying unoccupied orbitals. Its U═N bonding orbitals, formed by U(*f*) and N(*p*), occur in a region of the relatively low energy. Upon varying the ***axial*** substituent from H to ^{t}Bu and Ph, the U═N bonding orbitals of **2^{t}Bu** and **2Ph** are greatly destabilized. We further compared the U═E (E = N and O) bonds of **2H** with **3H** and their uranyl analogues, to address effects of the ***equatorial*** tetrahydrofuran (THF) ligand and the E group. It is found that the U═N bonds are slightly weaker than the U═O bonds of their uranyl analogues. This is in line with the finding that *cis*-UNR_2 isomers, although energetically unfavorable, are more accessible than *cis*-UO_2 would be. It is also evident that **2H** and **3H** display lower U═(NH) stretching vibrations at 740 cm^{-1} than the U═O at 820 cm^{-1} of uranyl complexes. With the inclusion of both solvation and spin−orbit coupling, the free energies of the formation reactions of the *bis*-imido uranium complexes were calculated. The formation of the experimentally synthesized **3Me**, **3Ph**, and **2^{t}Bu** are found to be thermodynamically favorable. Finally, the absorption bands previously obtained from experimental studies were well reproduced by time-dependent density functional theory calculations.

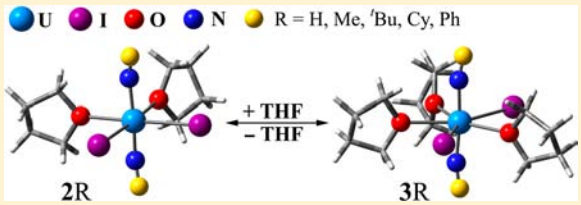

1. INTRODUCTION

Uranium has been widely used in nuclear weapons for defense and deterrent purposes and in nuclear reactors for energy production and medicine.[1−5] The hexavalent uranyl dication (UO_2^{2+}) is the most prevalent and the most thermodynamically stable form of uranium in these processes. Its solubility and mobility has led to growing concerns about waste management and environmental impact.[1−4,6−9] The uranyl ion is extraordinarily chemically robust because of the strongly covalent nature of the axial U═O bonds,[10] which makes its coordination chemistry much more active in the equatorial plane,[11−20] although its axial chemistry has been developed recently through uranyl oxo functionalization (-$SiMe_3$, -B-$(C_6F_5)_3$)[21−24] and cation−cation interaction (uranyl interaction with actinyl, and ions of alkaline metals, transition metals, and rare earth metals).[25−31]

Many analogues of the uranyl ion, such as complexes containing terminal imido (═NR), phosphorane iminato (═N-PR_3), phosphinedene (═PR), and methylidene (═CR_2) groups have been reported.[32−57] Unlike the axially inert uranyl complexes, the electronic structures of such complexes are easily tuned by varying their axial R groups. Moreover, it has been found that *bis*(imido) uranium(VI) complexes, for instance, exhibit both *cis*- and *trans*-configurations,[32,40] whereas only *trans*-uranyl complexes are experimentally known.[58] For example, a large number of *trans-bis*(imido) uranium(VI) complexes with the general formula of *trans*-$U(NR)_2(X)_n(Y)_m$ ($n \leq 3$, $m = 2$, $n + m = 4-5$) have been synthesized by Boncella's group.[40−49] The axial substituents (R) employed in these complexes have been mainly restricted to the methyl, *tert*-butyl, phenyl, and alkyl phenyl groups. In contrast, the equatorial ligands (X and Y) are highly diversified, including ligands with coordination of nitrogen atoms (pyridine and

Received: June 6, 2013
Published: July 8, 2013

disubstituted bipyridyl groups), chalcogen atoms (tetrahydrofuran (THF), $OPPh_3$, OTf, SPh, SePh and TePh), and halogen atoms (Cl, Br, and I). These studies were aimed at determining facile synthetic routes to the imido complexes as well as determining their reactivity, structure, and transformation into lower valent U(V) species.

Given the constraints imposed on experimental actinide chemistry by their chemical toxicity, radioactivity, and scarcity, computational techniques are an increasingly important tool in their study.[10,59−63] The correct description of electron correlation effects, relativistic effects of the heavy metal, and environmental effects is essential to accurately calculating properties of actinide complexes. Our previous studies on polypyrrolic actinide complexes and other systems indicated that the present quantum chemistry calculations can accurately predict the structural and electronic properties of actinide complexes as well as their reaction and ionization energies.[64−67]

In this work, a series of *trans-bis*(imido) uranium(VI) complexes, including experimentally known ones as well as theoretically designed (in silico) ones were examined using relativistic density functional theory (DFT). The axial R terminating groups have been systematically varied from H to methyl (Me), *tert*-butyl (^{t}Bu), cyclohexyl (Cy), and phenyl (Ph) groups. The steric and electronic structure changes induced by varying these imido substituents can be used in tuning the chemistry of the uranium center to which they are bound. This sort of chemistry is completely unavailable for the hexavalent uranium oxo analogues. We have also investigated the absorption spectra of the *bis*-imido complexes. Finally, the reaction energies leading to the formation of the experimentally synthesized imido complexes were discussed.

2. COMPUTATIONAL DETAILS

In this work, we have investigated three kinds of *trans-bis*(imido) uranium(VI) complexes, $U(NR)_2(THF)_2(cis\text{-}I_2)$ (**2R**), $U(NR)_2(THF)_3(trans\text{-}I_2)$ (**3R**), and $U(N^tBu)_2(THF)_3(cis\text{-}I_2)$ (**3^{t}Bu′**), where the R substituent is systematically changed from H, Me, ^{t}Bu, Cy, to Ph groups. The introduction of an additional THF ligand into the equatorial region between two iodine atoms of **2R** leads to a *trans*-I_2 configuration in **3R** (see Figure 1). Of these complexes, the **2^{t}Bu**, **3Me** and **3Ph** complexes have been experimentally synthesized.[40,41,49] For the $U(NR)_2(THF)_3(I_2)$ series of complexes with an equatorial *cis*-I_2 configuration, we performed calculations only on the experimentally known complex **3^{t}Bu′**.[41] For comparison, we also calculated the uranyl analogues of these *bis*-imido species, $UO_2(THF)_2(cis\text{-}I_2)$ (**2UO$_2$**), $UO_2(THF)_3(trans\text{-}I_2)$ (**3UO$_2$**), and $UO_2(THF)_3(cis\text{-}I_2)$ (**3UO$_2$′**), at the same level of theory.

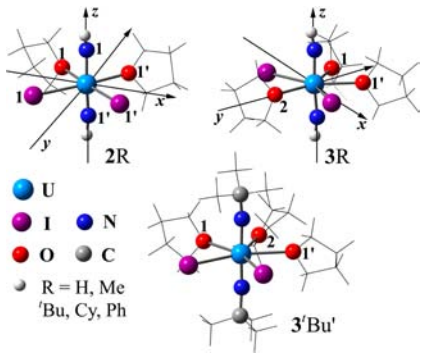

Figure 1. Optimized structures of *trans-bis*(imido) uranium(VI) complexes, $U(NR)_2(THF)_2(cis\text{-}I_2)$ (**2R**), $U(NR)_2(THF)_3(trans\text{-}I_2)$ (**3R**), and $U(N^tBu)_2(THF)_3(cis\text{-}I_2)$ (**3^{t}Bu′**). Atoms of the same type are numbered.

The geometries of *bis*-imido uranium complexes and their uranyl analogues were fully optimized in the gas phase without any symmetry constraints while using the Priroda code (Version 6).[68−72] Frequency calculations were used to confirm the local minima nature of the stationary points on the potential energy surface and also to estimate thermodynamic data. The vibrational spectra of the complexes were simulated by using Lorentzian broadening of the calculated IR frequencies and oscillator strengths. Population-based (Mayer)[73] bond orders were calculated. These calculations were carried out with the generalized gradient approximation (GGA) PBE functional,[74] and an all-electron correlation-consistent Gaussian basis sets of triple-ζ polarized quality for the large component and corresponding kinetically balanced basis sets for the small component (labeled as L2).[69] Relativistic effects were implemented using a scalar relativistic four-component all-electron (AE) approach,[71,75] which is based on the full Dirac equation but with spin−orbit projected out[76] and neglected. The use of a scalar-relativistic all-electron approach should be sufficient in describing the structural properties of the U(VI) species studied in this work.[59,77]

To consider the effects of solvation and spin−orbit coupling on the electronic structures and bonding in these complexes, single-point calculations were carried out with the ADF 2010.02 code[78−80] while employing the gas-phase optimized geometries. The atomic charges were also obtained. (See Table S2, Supporting Information, and accompanying text for a detailed discussion of charges calculated with different methods.) An integration parameter of 6.0 was applied. The solvent effects of THF were taken into account with the COSMO model as implemented in ADF.[81] Klamt radii were used for the main group atoms (H = 1.30 Å, C = 2.00 Å, N = 1.83 Å, O = 1.72 Å, and I = 2.38 Å)[82] and for the uranium atom (1.70 Å).[64−67,83] The scalar and spin−orbit coupled ZORA relativistic approach of van Lenthe et al[84−87] was employed, associated with the all-electron Slater-type TZP basis sets. Two functionals, GGA-PBE and hybrid-B3LYP,[88−91] were used in these calculations. Finally, electronic transitions in the THF solvent were calculated using time-dependent density functional theory (TDDFT) and different functionals (PBE, PBE0,[92,93] and B3LYP).

3. RESULTS AND DISCUSSION

3.1. Structures. *3.1.1. Geometry Structures.* The optimized structures of *trans-bis*(imido) uranium complexes (**2R**, **3R**, and **3^{t}Bu′**; R = H, Me, ^{t}Bu, Cy and Ph) obtained at the PBE/L2/AE level have been depicted in Figure 1. Some selected geometry parameters, bond orders, and atomic charges are listed in Tables 1−2 and Supporting Information, Tables S1 and S2. The experimental structural parameters of the synthesized complexes (**2^{t}Bu**, **3Ph**, and **3^{t}Bu′**)[40,41] as well as the calculated parameters of their uranyl analogues (**2UO$_2$**, **3UO$_2$**, and **3UO$_2$′**) are presented in Table 1.

The geometries of **2R** (octahedral) and **3R** (pentagonal bipyramidal) are consistent with the number of equatorial groups. The two imido ligands in these complexes are *trans* to each other with calculated N═U═N angles between 165° and 180° (Table 1). The N═U═N angles in **2^{t}Bu**, **3Ph**, and **3^{t}Bu′** were calculated to be 175.2°, 174.5°, and 173.1°, respectively, in good agreement with the experimental values of 175−177°.[40,41] The N═U═N angle of **3R** is closer to 180° than that of the respective **2R** counterpart. The calculated axial U═N-R angles range from 155° to 173°.

The U═N bond lengths were calculated as 1.88 Å for **2R** (R = H, Me, ^{t}Bu, and Cy) and slightly longer, 1.91 Å, for **2Ph** (Table 1). The U═N bonds in the corresponding **3R** and **3^{t}Bu′** complexes are generally of similar length, 1.87−1.90 Å. Compared with the experimental crystal structures,[40,41] the deviations between the calculated and experimental U═N

dx.doi.org/10.1021/ic401440w | Inorg. Chem. 2013, 52, 9143−9152

Table 1. Optimized Geometry Parameters for $U(NR)_2(THF)_2(cis\text{-}I_2)$ (2R, R = H, Me, ^{t}Bu, Cy and Ph), $U(NR)_2(THF)_3(trans\text{-}I_2)$ (3R), and $U(N^tBu)_2(THF)_3(cis\text{-}I_2)$ ($3^tBu'$) Complexes As Well As Uranyl Analogous $UO_2(THF)_2(cis\text{-}I_2)$ ($2UO_2$), $UO_2(THF)_3(trans\text{-}I_2)$ ($3UO_2$), and $UO_2(THF)_3(cis\text{-}I_2)$ ($3UO_2'$) in the Gas Phase, Compared with Experimental Values of 2^tBu, 3Ph, and $3^tBu'$[a]

		U=E[b]	U–I	U–O1	U–O2	N–H/C	E=U=E[b]	U=N–H/C
Cal.	**2H**	1.875	3.001	2.477		1.025	168.5	155.3
	2Me	1.878	3.011	2.492		1.444	170.8	163.8
	2^{t}Bu	1.877	3.028	2.504		1.476	175.2	161.8
	2Cy	1.880	3.022	2.495		1.456	171.0	163.4
	2Ph	1.913	2.986	2.474		1.388	165.6	168.8
	3H	1.870	3.139	2.542	2.470	1.025	173.5	167.1
	3Me	1.875	3.144	2.556	2.477	1.442	174.4	172.0
	3^{t}Bu	1.882	3.145	2.592	2.536	1.477	175.5	172.6
	3Cy	1.877	3.143	2.574	2.486	1.455	179.2	167.4
	3Ph	1.901	3.125	2.546	2.448	1.390	174.5	170.1
	3^{t}Bu′	1.889	3.063	2.639	2.665	1.477	173.1	164.6
	2UO$_2$	1.797	2.995	2.468			−168.0	
	3UO$_2$	1.794	3.124	2.537	2.439		−176.3	
	3UO$_2$′	1.799	3.049	2.576	2.623		−167.8	
Expt.[c]	**2^{t}Bu**	1.844	3.054	2.415			175.4	168.3
	3Ph	1.863	3.130	2.458	2.418		177.4	177.0
	3^{t}Bu′	1.855	3.137	2.490	2.534		175.6	166.3

[a]Bond lengths in Å and angles in degree. [b]E denotes the N atoms for **2R**, **3R**, and **3^{t}Bu′**, and the O atoms for **2UO$_2$**, **3UO$_2$**, and **3UO$_2$′**. [c]Experimental values of **2^{t}Bu**, **3Ph**, and **3^{t}Bu′** from refs 40,41.

Table 2. Atomic Charges for 2R, 3R and $3^tBu'$ (R = H, Me, ^{t}Bu, Cy, and Ph) As Well As $2UO_2$, $3UO_2$ and $3UO_2'$ Calculated at the ADF: PBE/TZP/ZORA/COSMO Level

	U	E[a]	UE$_2$[a]	I	O1	O2
2H	0.985	−0.326	0.333	−0.283	−0.663	
2Me	0.825	−0.414	−0.003	−0.307	−0.668	
2^{t}Bu	0.651	−0.360	−0.069	−0.303	−0.677	
2Cy	0.575	−0.369	−0.163	−0.299	−0.675	
2Ph	0.599	−0.334	−0.069	−0.214	−0.676	
3H	1.137	−0.312	0.513	−0.433	−0.641	−0.628
3Me	0.942	−0.429	0.085	−0.447	−0.647	−0.634
3^{t}Bu	0.989	−0.396	0.197	−0.416	−0.651	−0.645
3Cy	0.750	−0.385	−0.019	−0.437	−0.655	−0.639
3Ph	0.650	−0.335	−0.019	−0.360	−0.652	−0.642
3^{t}Bu′	0.758	−0.413	−0.068	−0.300	−0.654	−0.652
2UO$_2$	1.253	−0.605	0.043	−0.195	−0.673	
3UO$_2$	1.410	−0.630	0.150	−0.348	−0.649	−0.634
3UO$_2$′	1.221	−0.644	−0.066	−0.217	−0.649	−0.651

[a]E denotes the N atoms for **2R**, **3R**, and **3^{t}Bu′**, and the O atoms for **2UO$_2$**, **3UO$_2$**, and **3UO$_2$′**.

bond lengths for **2^{t}Bu**, **3Ph**, and **3^{t}Bu′** are generally less than 0.04 Å. The computed U=N bond orders in these complexes range from 2.09 to 2.32 (Supporting Information, Table S1). The magnitudes of these bond orders (greater than 2.0) indicate the presence of partial triple bond character. In general the **2R** complexes have slightly smaller U=N bond orders than their counterpart **3R** species. The bond orders of U=N in the imido complexes are smaller than those of the U=O bonds in their analogous uranyl complexes.

Herein, we will discuss the Mulliken atomic charges of complexes in solution which were calculated at the PBE/TZP/ZORA level with the ADF code while employing the COSMO model (Table 2; see also Supporting Information, Table S2 and accompanying discussion). The charges on the uranium atoms were found to be smaller in *bis*-imido uranium complexes than those in the corresponding uranyl complexes. This would to some extent indicate more covalent character in the U=N bonds. This agrees with previous theoretical results.[41,47,48,61] The uranium charges of **2R** were calculated to decrease with the increase of the donating ability of R from H, Me, to ^{t}Bu. **2Ph**, having a conjugative and donating phenyl substituent, exhibits an even smaller uranium charge. A similar trend is reproduced in **3R** with the exception of **3^{t}Bu**. In short, the variation of the axial substituent in the *bis*-imido uranium complexes has a rather strong effect on the partial charges on the uranium and UN_2 groups. This feature of the *bis*-imido complexes suggests the possibility of tuning their electronic properties by modifying the axial R substituent. As an example, the charge on the uranium center might indicate its susceptibility to equatorial coordination of neutral or anionic ligands.

One may note that both *trans*- and *cis*-*bis*(imido) uranium(VI) complexes, such as *trans*-$[U(N^tBu)_2(THF)_2(cis\text{-}I_2)]$ (**2^{t}Bu**), *trans*-$[U(N^tPh)_2(THF)_3(trans\text{-}I_2)]$ (**3Ph**), and *cis*-$[U(NPh)_2(C_5Me_5)_2]$, have been experimentally synthesized.[32,34,35,40,41] This suggests that the RN=U=NR linkage is much softer than the U=O=O one which has not been found to form the *cis*-configuration except in a number of theoretical reports.[67,94] In this work, we have also optimized possible structures for *cis*-$[U(N^tPh)_2(THF)_2(cis\text{-}I_2)]$ (*cis*-**2Ph**) and *cis*-$[U(N^tPh)_2(THF)_3(trans\text{-}I_2)]$ (*cis*-**3Ph**), Supporting Information, Figure S1. The total energies of *cis*-**2Ph** and *cis*-**3Ph** were calculated to be 7.6−9.0 and 10.7−14.8 kcal/mol higher than those of the *trans*-isomers **2Ph** and **3Ph**, respectively, Supporting Information, Table S3. This demonstrates that the *cis*-isomers are energetically unfavorable although they might be accessible under some circumstances, which is consistent with their experimental synthesis.[40,41]

3.1.2. Vibrational Structure. For a series of *cis*-*bis*(imido) uranium complexes, Burns et al.[34] have assigned two kinds of characteristic bands, ν(U=N) at 888−917 cm^{-1} and ν(N−C) at 1247−1302 cm^{-1}. In Boncella's studies,[40,41] bands measured

dx.doi.org/10.1021/ic401440w | Inorg. Chem. 2013, 52, 9143−9152

at 1170 cm^{-1} for **2^{t}Bu** and 1270 cm^{-1} for **3Ph** were attributed to the U═N vibrational mode coupled out of phase with the N−C stretching. To provide a clear understanding of the U═N and N−C vibrations, we have calculated frequencies of *bis*-imido complexes (**2R**, **3R**, and **3^{t}Bu′**) as well as their uranyl analogues (**2UO$_2$**, **3UO$_2$**, and **3UO$_2$′**), Figure 2 and Supporting Information, Figures S2−S4.

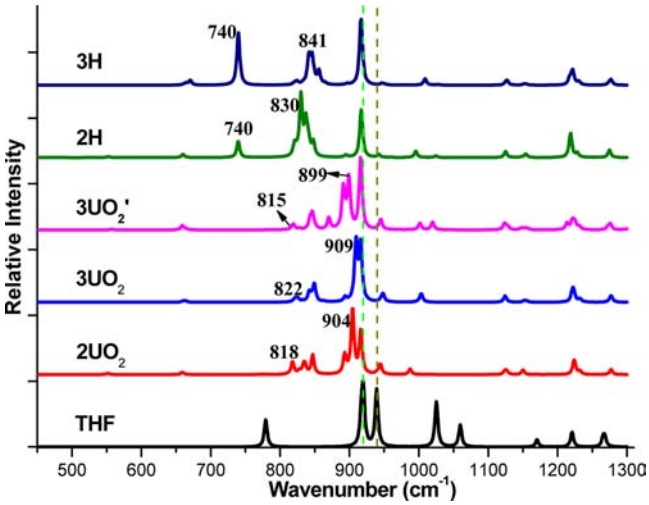

Figure 2. Simulated vibrational spectra of THF, $UO_2(THF)_2$(*cis*-I_2) (**2UO$_2$**), $UO_2(THF)_3$(*trans*-I_2) (**3UO$_2$**), $UO_2(THF)_3$(*cis*-I_2) (**3UO$_2$′**), $U(NR)_2(THF)_2$(*cis*-I_2) (**2H**), and $U(NH)_2(THF)_3$(*trans*-I_2) (**3H**). For convenient comparison, all the spectra are normalized.

In the *bis*-imido uranium complexes, perturbations by the axial R groups make the U═NR (R = H, Me, ^{t}Bu, Cy and Ph) vibrations more complicated than the U═O stretching modes found in the uranyl complexes. We start with the simplest model complexes, **2H** and **3H**, *bis*-imido complexes with axial hydrogen atoms. They were calculated to show bands at 740/830 and 740/841 cm^{-1}, respectively, Figure 2. The bands at 740 cm^{-1} are comparable to the experimental value of 752 cm^{-1} for the $N{\equiv}U^{V}{=}NH$ molecule prepared in solid argon.[95] On the whole, these calculated U═NH frequencies of the imido complexes are lower than the U═O stretches found in the uranyl complexes. This correlates well with the fact that the imido complexes display longer U═N distances (Table 1) and smaller bond orders (Supporting Information, Table S1) than their analogous uranyl complexes.

In contrast to the uranimine complexes such as $N{\equiv}U^{V}{=}NH$,[95] **2H** and **3H**, there is strong coupling between the U═N and N-R bonds in the **2R** and **3R** complexes where R is Me, ^{t}Bu, Cy, and Ph. Regarding **2R**, the U═N-R stretching vibrational band of **2Me** was calculated to be 1181 cm^{-1}, as well as 1059 cm^{-1} for **2^{t}Bu** and 1261 cm^{-1} for **2Ph** (Supporting Information, Figure S2). These changes are most likely related to electronic effects and steric effects of the axial R groups, as depicted by the UN-R bond lengths. The phenyl group is known to have greater electronic conjunction effects. For example, **2Ph** was calculated to have longer U═N and shorter N−C bond lengths (1.912 and 1.388 Å) than **2Me** (1.878 and 1.444 Å). The calculated bond orders also attest to this effect, 2.09 (U═N) and 1.21 (N−C) for **2Ph** and 2.29 and 1.02 for **2Me**. Thus, the stronger coupling in U═N-Ph compared to U═N-Me rationalizes that **2Ph** has a larger U═N-R frequency than **2Me**. From the point of view of bond lengths and bond orders, **2^{t}Bu** is supposed to have a U═N-R frequency close to that of **2Me**. However, considering the much bigger size of ^{t}Bu than Me, it is not surprising to obtain an even smaller U═N-^{t}Bu stretching vibrational frequency of **2^{t}Bu**.

Similarly, the **3R** (R = Me, ^{t}Bu, Cy and Ph) complexes also display the U═N-R modes in the 1021−1260 cm^{-1} region (Supporting Information, Figure S3). The band of the complex **3Ph** was calculated to be at 1260 cm^{-1}, agreeing well with the experimental value of 1270 cm^{-1},[40,41] and comparable to the range of 1247−1302 cm^{-1} for a series of synthesized *cis-bis*(aryl imido) uranium complexes.[34]

3.1.3. Electronic Structures. The electronic properties of *bis*-imido uranium complexes in THF solution were examined at the B3LYP level while employing the TZP basis sets, the scalar relativistic ZORA approach, and the COSMO solvation model. Complexes **2R** including **2H**, **2Bu**, and **2Ph** will be discussed to reveal the effects of ***axial*** substituents on electronic structures. Then, effects of the ***equatorial*** THF ligands are taken into account by comparison of **2H** and **3H**. Also the difference of U═E (E = N and O) bonds is addressed by investigating **2H** and **2UO$_2$** as well as **3H** and **3UO$_2$**.

In Figure 3, we illustrate the energy-correlation diagrams of the characteristic orbitals of **2H**, **2^{t}Bu**, and **2Ph**. More orbital

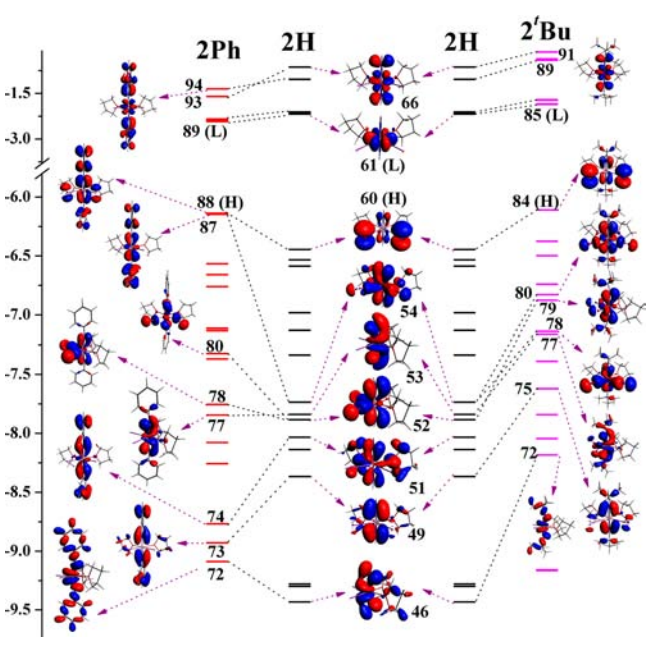

Figure 3. Energy-correlation diagrams of typical orbitals of U(*f*), π(I) and U═N bond for **2H**, **2^{t}Bu**, and **2Ph** from the B3LYP/TZP/ZORA/COSMO calculations, where the energy levels of **2H** are shown twice to clarify the correlation diagrams.

diagrams are given in Supporting Information, Figures S5−S7, compared with detailed composition information in Supporting Information, Tables S4−S6.

Our calculated results reveal that **2H**, **2^{t}Bu**, and **2Ph** have very similar unoccupied orbitals. Their four low-lying unoccupied orbitals, for instance, are of U(*f*)-character. This is generally typical of hexavalent uranium complexes. The π^*(U═N) *anti*-bonding orbitals are found at about 0.74−1.30 eV further in the virtual band than the U(*f*) orbitals. The complexes however differ in the characters of their occupied orbitals. For example, **2H** exhibits six high-lying iodine-based occupied orbitals (HOMO to HOMO-5); several U═N

dx.doi.org/10.1021/ic401440w | *Inorg. Chem.* 2013, 52, 9143−9152

bonding orbitals occur in the subsequent lower-energy region, accompanied by orbitals of THF character. Its HOMO (orbital 60) is an *anti*-bonding combination of π(I) and π(U═N), containing 86.8% p_z(I), 4.2% f_{xyz},d_{xz}(U), and 8.6% p_x(N). Orbitals 51, 52, and 54 have π(U═N) bonding character, arising from the f(U) and p(N) combination. Orbital 49 is also of π(U═N) character, but with some d_{xz}(U) participation. Combined σ and π U═N bonding is found in orbitals 46 and 53.

The variation from H to ^{t}Bu allows for the tuning of the electronic structures of *bis*-imido uranium complexes. The U═N bonding orbitals of **2^{t}Bu** such as 72, 75, and 77−80 were calculated to be higher than respective correlated orbitals of **2H**, Figure 3. These U═N bonds display similar electron-density shape, but different quantitative composition of orbitals. The ^{t}Bu group in **2^{t}Bu** shows stronger participation than the H in **2H**. This causes the U═N bonding orbitals of **2^{t}Bu** to energetically rise, and consequently leads to weakening of its U═N bonds. However, the calculated U═N distance and bond order of **2^{t}Bu** (Table 1 and Supporting Information, Table S1) are only a little longer (0.002 Å) and smaller (0.03) than the ones of **2H**, respectively. This can be rationalized by the electron-donating and steric effects of the ^{t}Bu group. First, the strong electron-donating ability of *tert*-butyl enhances the U═N bonding of **2^{t}Bu**, readily generating a shorter U═N distance and larger bond order. On the other hand, the steric effect weakens the U═N bonding to decrease the repulsion interaction of big groups, and gives rise to a longer distance and smaller bond order. Consequently, **2^{t}Bu** shows approximately the same bond length and bond order as those of **2H**. Additionally, it is worth pointing out that the steric effect of *tert*-butyl plays a more important role than its electron-donating ability, because electronic structures reveal relatively weak U═N bonding of **2^{t}Bu**.

Complex **2Ph** shows interesting electronic structure features with respect to the model complex **2H**. The axial Ph group greatly participates in the high-lying occupied orbitals. For example, 48.5% and 53.2% p_x(Ph) are found in HOMO and HOMO-1, respectively. Obviously, the electronic properties of the phenyl groups match those of the U═N bonds very well. The U═N bonding orbitals of **2Ph** are also located in the high-energy region relative to those of **2H**, similar to the cases in **2^{t}Bu**. Differently, the rising of the highest-energy U═N bonding orbital of **2Ph** (i.e., 87, HOMO-1) relative to the correlated one of **2H** (orbital 54) is much greater than that of **2^{t}Bu** (80, HOMO-4). Figure 3 shows that orbital 87 of **2Ph** is of π(U═N)-type, composed of 15.5% f_{z^2x}(U), 17.1 p_x(N) as well as 53.2% p_x(Ph). It is about 1.59 eV higher than orbital 54 of **2H** with the same π(U═N) character but with little involvement of the axial H substituents. Correspondingly, a smaller energetic rising (0.91 eV) is found from orbital 80 of **2^{t}Bu** to orbital 54 of **2H**. Therefore, the analysis of the electronic structures proves weaker U═N bonding of **2Ph** than those of not only **2H** but **2^{t}Bu** as well. Moreover, this also agrees well with the obviously longer bond length (1.91 Å) and smaller bond order (2.09) of **2Ph** than those of **2H** (1.88 Å and 2.31). Apart from the U═N-dominant orbitals, more π(U═N) contribution is found in the HOMO of **2Ph** than in HOMOs of **2H** and **2^{t}Bu**. In brief, it is the increased phenyl contribution in the high-lying occupied orbitals such as HOMO-1 and HOMO that results in weaker U═N bonds of **2Ph**. The variation of axial substituents from H to ^{t}Bu and Ph can tune the electronic structures of formed *bis*-imido uranium complexes.

Energy-correlation diagrams of characteristic orbitals of **2H** and **3H** are illustrated in Figure 4 and compared with those of

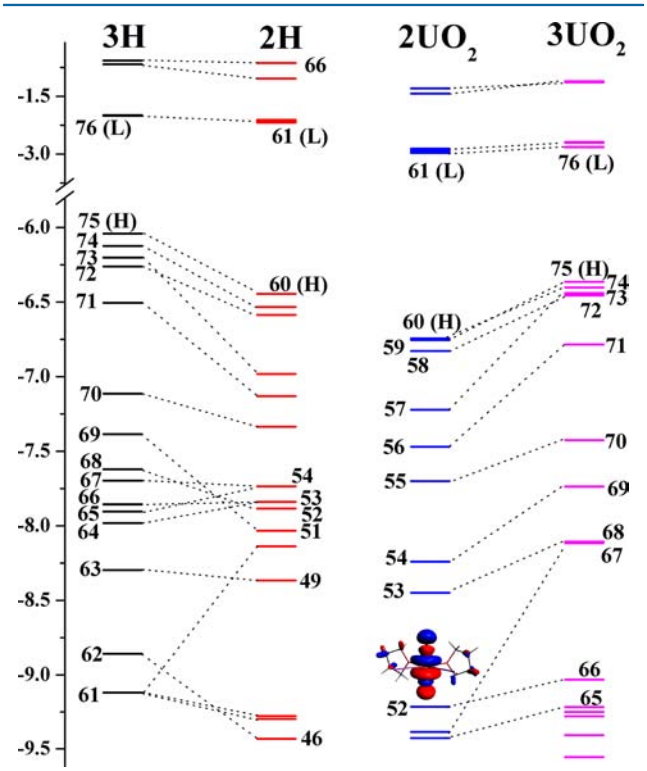

Figure 4. Energy-correlation diagrams of typical orbitals of U(f), π(I), and U═N bond for **2H**, **3H**, **2UO$_2$**, and **3UO$_2$** from the B3LYP/TZP/ZORA/COSMO calculations.

2UO$_2$ and **3UO$_2$**. Detailed composition information is given in Supporting Information, Tables S7−S9. These results reveal that all the complexes feature low-energy and energetically close unoccupied orbitals with U(f)-character, but differ in their occupied orbitals. Complex **3H** shows very similar order and character of occupied orbitals as those of **2H** in Figure 4 and Supporting Information, Table S7, but has relatively weak U═N bonds. With respect to uranyl complexes, the high-lying filled orbitals of **2UO$_2$** and **3UO$_2$** are predominantly iodine and THF-based. Their highest-lying U═O bonding orbital is of σ character involving 41% $5f_{z^3}$ and 11% $6p_z$ of uranium (mean value). Moreover, the orbitals of U═O bonds of these uranyl complexes were calculated to be energetically lower than the U═N bonding ones of *bis*-imido complexes. This suggests that the U═N bonds are weaker than the U═O ones, as also evidenced by the former having longer bond lengths, smaller bond orders, and lower stretching vibrational frequencies.

Finally, from a structural view of point, **2H** could adopt C_s symmetry. Thus, starting from the Priroda-optimized geometry, we have symmetrized **2H** to form a new structure **2H′** with C_s symmetry. The two structures **2H** and **2H′** are compared in Supporting Information, Figure S8. It is found that the differences in orbital composition and energies are negligible. Moreover, their electronic spectra are also similar.

3.2. Absorption Spectra. The electronic absorption spectra of the *bis*-imido complexes were calculated using TDDFT. In this work we compared the performance of hybrid and GGA functionals (PBE, PBE0[92,93] and B3LYP), examined the effect of spin−orbit coupling on the calculated spectra, and explored the effect of the axial R substituent by comparing the

dx.doi.org/10.1021/ic401440w | *Inorg. Chem.* 2013, 52, 9143−9152

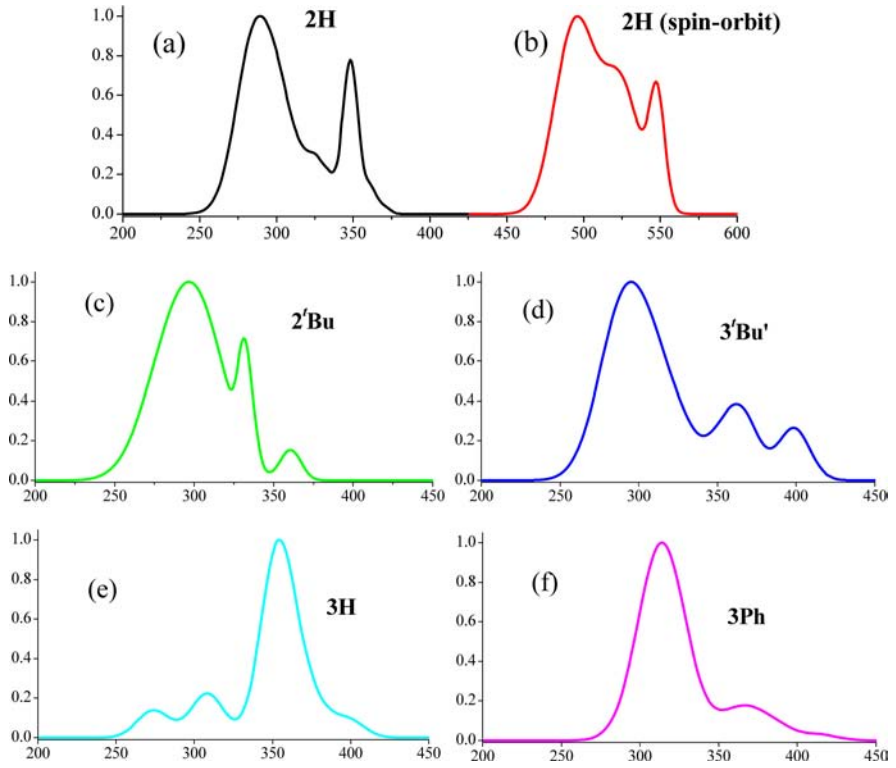

Figure 5. Simulated absorption spectra in THF for *bis*-imido complexes from the TD-B3LYP/TZP/ZORA/COSMO calculations, where **2H** was also calculated with the inclusion of spin−orbit coupling (b). For convenient comparison, all the spectra are normalized.

Table 3. Calculated Absorptions of 2H in the THF Solution at the TD-B3LYP/TZP/ZORA/COSMO Level

λ (nm)[a]		λ (nm)[b]	E (eV)[b]	f[c]	configurations[d]	weight > 0.1	expt.[e]
Band I	349	351	3.53	0.0224	59→61	0.6278	353 (2200)
					60→64	0.2407	
		346	3.58	0.0246	58→64	0.8617	
Band II	326	327	3.79	0.0047	55→61	0.2935	
					56→62	0.1752	
					52→61	0.1522	
					53→64	0.1425	
		324	3.82	0.0053	57→61	0.6447	
					55→61	0.1856	
Band III	290	305	4.07	0.0128	56→62	0.3077	291 (3500)
					52→61	0.2203	
					54→62	0.1062	
		292	4.25	0.0216	52→61	0.6885	
					55→61	0.1484	
		281	4.41	0.0271	52→62	0.3980	
					55→62	0.3677	

[a]The simulated absorption peak (nm). [b]Calculated absorption transitions in nm and eV. [c]Oscillator strength. [d]Orbitals 60 and 61 correspond to HOMO and LUMO, respectively. [e]Experimental absorption (nm) of **2^{t}Bu** from refs 40,41 and molar absorption coefficient (dm^3 mol^{-1}cm^{-1}) listed in parentheses.

calculated spectra to available experimental data. The experimental absorption spectrum of **2^{t}Bu** has absorption bands at 291 nm (molar absorptivity ε = 3500 dm^3·mol^{-1}·cm^{-1}) and 353 nm (ε = 2200 dm^3·mol^{-1}·cm^{-1}). The calculated absorption spectra (Supporting Information, Figure S9) illustrate that the TDDFT calculations with the B3LYP functional yield the best results. The PBE0 functional generally results in absorptions at lower wavelengths even though it also results in spectral patterns similar to experimental results.[40,41]

Given the above, the absorption spectra of the **3Ph** and **3^{t}Bu′** were also examined at the TD-B3LYP/TZP/ZORA/COSMO level. These complexes have been experimentally synthesized. The model complexes **2H** and **3H** were also studied, Figure 5. The composition and natures of the relevant transitions are listed in Table 3 and in Supporting Information, Tables S10–S13.

As seen in Figure 5a, the complex **2H** displays two strong peaks and one shoulder peak. ***Band I*** at 349 nm is made up of two transitions, one at 346 nm and the other at 351 nm, Table 3. This band is assigned as being primarily of $\pi[p(\mathrm{I})]\rightarrow f(\mathrm{U})$

dx.doi.org/10.1021/ic401440w | *Inorg. Chem.* 2013, 52, 9143−9152

character, modified by a small amount of π(U═N)→f(U) transition (Supporting Information, Table S4 and Figure 3). The shoulder peak at around 326 nm (labeled ***Band II***) is of $\pi[p_x, p_y(\mathrm{I})]$→$f$(U) transition character, similar to that of ***Band I***. The transitions ranging from 281 to 305 nm form a strong peak at 290 nm (***Band III***). These transitions are mainly of π(U═N)→f(U) character albeit with some minor p(I)→f(U) character. For example, the transition at 292 nm has contributions from two electronic excitations (52→61, 69% and 55→61, 31%). Orbital 52 is composed of 25.7% f_{z^2y}(U) and 50.6% p_y(N) forming the π(U═N) bond. Orbital 61 (LUMO) is essentially an empty $f_{x(x^2-3y^2)}$ orbital on the uranium center. This allows us to assign the absorption at 292 nm to a π(U═N)→f(U)-type transition.

3H, **2^{t}Bu**, **3Ph**, and **3^{t}Bu′** all exhibit these three characteristic absorption bands within the range of 250−450 nm (Supporting Information, Tables S10−S13). The first two low-energy bands, ***Bands I*** and ***II***, have p(I)→f(U) character with a slight amount of π(U═N)→f(U) modification while the high energy ***Band III*** is of π(U═N)→f(U) character with minor p(I)→f(U) character. For **2^{t}Bu** and **3Ph**, the calculated peaks at 297/360 and 314/360 nm respectively are in good agreement with the experimentally reported absorptions at 291/352 nm.[40,41]

To obtain accurate electronic spectra for actinide species, it is generally thought that the effects of spin−orbit coupling and dynamic electron correlation have to be included. The latter effect can be included by using complete active space second-order perturbation theory (CASPT2). However, as a result of the steep computational scaling with the size of the active space, this approach is often limited to small actinide molecules in the gas phase.[63,96−98] We have performed a spin−orbit TDDFT calculation on **2H** to examine the effect of spin−orbit coupling on the calculated electronic spectra. It is shown in Figures 5a and 5b that, while the scalar relativistic and spin−orbit coupled TDDFT calculations give similar general absorption spectra patterns, the inclusion of spin−orbit coupling effect causes a red-shift.[99,100]

3.3. Reaction Energies. Boncella and co-workers have synthesized **2^{t}Bu** and **3Ph** in a high yield using the reaction given below.[40,41] The same group has recently reported the synthesis of **3Me** by using a $[\mathrm{U(NMe)_2(THF)_4I}]\mathrm{I_3}$ precursor.[49]

$$\mathrm{UI_3(THF)_4 + 2RNH_2 + 1.5I_2 + 4NEt_3} \rightleftharpoons \mathbf{nR} + \mathrm{4NEt_3HI + (4-}n\mathrm{)THF}$$

(n = 2 and 3; R = H, Me, ^{t}Bu, Cy, and Ph)

Solvation effects have been shown to be important in obtaining accurate reaction energies involving actinide species.[64−67] In addition to this, as the given formation reaction involves the transformation of a trivalent reactant to a hexavalent product, spin−orbit coupling effects may also play a significant role. Thus, we list in Supporting Information, Table S14 the obtained solvation (G_{sol}) and spin−orbit (G_{so}) free energies of each complex as well as their contributions (ΔG_{sol} and ΔG_{so}) to the total reaction energies. It is found that the calculated ΔG_{sol} is much greater than ΔG_{so}, suggesting solvation is more important than spin−orbit in calculations of reaction energies.

In Table 4, the calculated thermodynamic energies in the gas phase and THF solution are presented. The free energies of reaction obtained with the B3LYP functional while including both solvation and spin−orbit coupling effects,

Table 4. Calculated Energies (kcal/mol) of Formation Reactions of 2R, 3R, and 3^{t}Bu′ (R = H, Me, ^{t}Bu, Cy and Ph)

$\mathrm{UI_3(THF)_4 + 2RNH_2 + 1.5I_2 + 4NEt_3} \rightleftharpoons \mathbf{nR} + \mathrm{4NEt_3HI + (4-}n\mathrm{)THF}$ (n = 2 and 3)

	Δ_rE(gas)[a]	Δ_rE_0(gas)[a]	Δ_rG(gas)[a]	Δ_rG(sol+so)$_{B3LYP}$[b]	Δ_rG(sol+so)$_{PBE}$[b]
2H	−36.88	−32.95	−22.81	−86.78	−78.74
2Me	−50.75	−47.98	−37.74	−101.68	−93.94
2Bu	−47.06	−43.69	−29.38	−92.52	−84.91
2Ph	−47.54	−44.54	−30.98	−90.51	−83.51
2Cy	−49.42	−46.62	−33.16	−96.75	−89.11
3H	−45.76	−41.21	−18.33	−77.85	−70.02
3Me	−59.85	−56.26	−33.37	−92.45	−84.87
3Bu	−53.01	−48.78	−20.18	−78.63	−71.00
3Ph	−57.92	−54.28	−29.75	−82.31	−75.73
3Cy	−57.32	−53.74	−27.46	−86.13	−78.70
3 ^{t}Bu′	−47.79	−43.66	−16.43	−79.83	−71.83

[a] Δ_rE(gas), Δ_rE_0(gas), and Δ_rG(gas) denote the total energy, total energy including zero-point vibration energy, and free energy of the reaction in the gas phase, respectively. [b] Δ_rG(sol+so) = Δ_rG(gas) + ΔG_{sol} + ΔG_{so}, $\Delta G_{sol} = \sum\nu_B G_{sol}(B)$ and $\Delta G_{so} = \sum\nu_B G_{so}(B)$, where $G_{sol}(B)$ and $G_{so}(B)$ are the calculated solvation and spin−orbit free energies of each complex (B) in the formation reaction, respectively. Two functionals, B3LYP and PBE, were used in the calculations, thus yielding $\Delta_rG(\mathrm{sol+so})_{B3LYP}$ and $\Delta_rG(\mathrm{sol+so})_{PBE}$, respectively.

$\Delta_rG(\mathrm{sol+so})_{B3LYP}$, are plotted in Figure 6. The corresponding scalar and spin−orbit coupling relativistic results obtained with

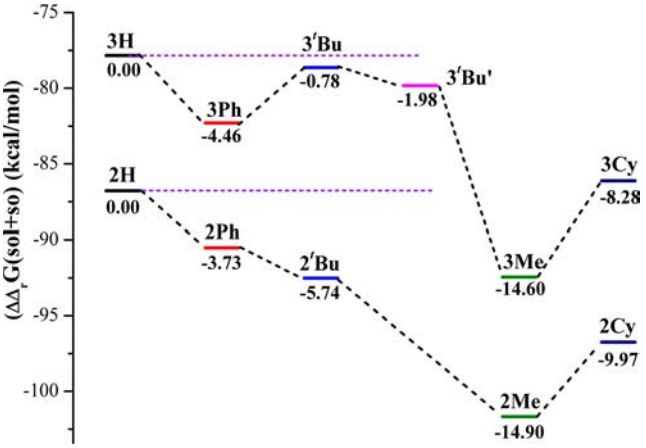

Figure 6. Free energies (kcal/mol) of formation reactions of **2R**, **3R**, and **3^{t}Bu′** (R = H, Me, ^{t}Bu, Cy, and Ph) in the THF solution, where the corresponding solvation and spin−orbit energies were calculated at the B3LYP level, together with values of reaction energies relative to those of **2H** and **3H**, respectively.

the PBE functional are presented in the Supporting Information, Figure S10. For the **3R** complexes, an exothermic process is found from **3H** to its alkyl or aryl substituted **3R**. Overall exothermic reaction energies of −14.60, −0.78, −8.28, −4.46, and −1.98 kcal/mol were calculated for **3R** (R = Me, ^{t}Bu, Cy, and Ph) and **3^{t}Bu′** relative to **3H**, respectively. From a thermodynamic point of view, the case of **3Me** is not surprising as it has been experimentally synthesized.[49] An exothermic process was calculated from **3^{t}Bu** to **3Ph**. A recent study on the imido exchange in *bis*(imido) uranium(VI) complexes has presented similar calculated results.[43] However, the transformation from **2^{t}Bu** to **2Ph**, equatorially coordinated by two

dx.doi.org/10.1021/ic401440w | *Inorg. Chem.* 2013, 52, 9143−9152

THF ligands, shows a reverse case, because the formation energy of the former is 2.01 kcal/mol lower. We conjecture that the electronic and steric effects of both substituents (^{t}Bu and Ph) and equatorial THF (two and three) result in this discrepancy. Intuitively, the *tert*-butyl group has a larger electron-donating ability than phenyl, and equatorial coordination with three THF ligands will show a higher steric effect. In **2^{t}Bu**, the donating property of the *tert*-butyl group plays the dominant role, and also the steric repulsion between *tert*-butyl and two equatorial THF would not be high. Consequently, **2^{t}Bu** appears slightly more stable than **2Ph**, where the former is featured with a relative short and strong U═N bond (1.88 Å with bond order 2.28) as well as moderate U−I (3.03 Å) and U−O(THF) (2.50 Å) bonds. In contrast, one additional THF is coordinated to **3^{t}Bu**, where the steric repulsion is turning stronger. And thus, because of having the relatively small steric effect of a phenyl and three THFs, **3Ph** turns out to be energetically favorable. It is worth noting that **2^{t}Bu** and **3Ph** were experimentally synthesized, supporting our calculated results.[40,41]

NMR measurements were carried out to monitor the solution reactions of **2^{t}Bu** and **3Ph** with excess THF.[40] Rapid exchange of coordinated and uncoordinated THF molecules was observed on the NMR time scale. This suggests that **2R** and **3R** with different solvates are probably simultaneously present in solutions. It appears that the **3R** complexes are favored because more of them have been isolated in the solid state.[40,41,49] However, the actual solution phase structures may be different. In the calculations (Table 3), $\Delta_rG(\mathrm{sol+so})_{\mathrm{B3LYP}}$ of the **2R** systems were calculated to fall within −86.78 and −101.68 kcal/mol, while those of **3R** are more positive. As far as these results are concerned, it appears that the **2R** complexes are more stable than **3R** in the solution. To elucidate the stability of **2R** and **3R**, we calculated the following THF exchange reaction and presented thermodynamical energies in Supporting Information, Table S15:

$$\mathbf{3R} \rightleftharpoons \mathbf{2R} + \mathrm{THF} \quad (\mathrm{R} = \mathrm{H, Me, {}^tBu, Cy, and Ph})$$

In the gas phase, the calculated $\Delta_rE(\mathrm{gas})$ and $\Delta_rH(\mathrm{gas})$ are positive, while $\Delta_rG(\mathrm{gas})$ is negative. Clearly, the former (internal energy and enthalpy) reflects that stuff sticks together in the gas phase. On the other hand, the negative values for the Gibbs free energies seem to be an entropy effect, one particle going to two particles. Apparently, the entropy wins. In solution, all the calculated free energies are negative. This can be understood qualitatively by considering differential solvation of the left and right-hand sides of the reaction. The solvation free energies of the large complexes **2R** and **3R** will be relatively similar; however, a small molecule with a large dipole moment such as THF will be strongly stabilized in polar solvents. Overall, solvation will shift the equilibrium to the right-hand side.

4. CONCLUSIONS

In this work, a series of *trans-bis*(imido) uranium(VI) complexes, **2R**, **3R**, and **3^{t}Bu′** (R = H, Me, ^{t}Bu, Cy to Ph), were examined using relativistic density functional theory. On the basis of these and additional calculations of the analogous **2UO$_2$**, **3UO$_2$**, and **3UO$_2$′**, as well as experimentally reported results of **2^{t}Bu**, **3Ph**, and **3^{t}Bu′**,[40,41] we come to the following conclusions.

These *trans-bis*(imido) species have linear/nearly linear N═U═N and U═N-R structural features. They are more energetically favorable than their corresponding *cis*-isomers, as shown by comparing calculations on **2Ph**/**3Ph** with those for *cis*-**2Ph**/*cis*-**3Ph**. The U═N bond lengths of *trans-bis*(imido) complexes were calculated to be within 1.87−1.91 Å, comparable to the experimentally measured 1.85−1.87 Å.[40,41] The bond orders of the U═N bonds indicate partial triple bonding character. The calculated atomic charges at the uranium center are changing with the variation of the axial R group in either **2R** or **3R**.

The simplest model complexes, **2H** and **3H**, display characteristic vibrational bands at 740/830 and 740/841 cm^{-1}, respectively, attributable to the symmetric/asymmetric U═(NH) stretching vibrational modes. The symmetric frequency is close to the experimentally reported 752 cm^{-1} U═(NH) vibration in N≡U^{V}═NH.[95] On going from H to larger axial R (R = Me, ^{t}Bu, Cy, and Ph) substituents, a strong coupling is generated between the U═N and N-R stretching vibrations.

The analysis of electronic structures has provided insight into the nature of the U═N bonds. **2H** is featured with iodine-based high-lying occupied orbitals and U(*f*)-type low-lying unoccupied orbitals. Its U═N bonding orbitals are formed by U(*f*) and N(*p*), being located in the relatively low-energy region. The electronic structures can be tuned by varying the ***axial*** substituent from H to R (R = Me, ^{t}Bu, Cy, and Ph). For example, the U═N bonding orbitals of **2^{t}Bu** and **2Ph** greatly rise in energy relative to those of **2H**, which results in weaker U═N bonding of the former, as well as longer bond lengths and smaller bond orders. The good match of phenyl group and U═N bonds in terms of orbital properties results in **2Ph** having the weakest U═N bonds among the three complexes. We also found that **3H** has relatively weak U═N bonds because of additional ***equatorial*** THF ligands. Similarly, the orbitals of the U═N bonds are energetically higher than those of the U═O bonds in analogous uranyl complexes, suggesting the U═N bonds are weaker than the U═O bonds.

Our TD-B3LYP/TZP/ZORA/COSMO calculations reveal the existence of three major bands in the absorption spectra of these *bis*-imido uranium species. The two low-energy bands were assigned to the *p*(I)→*f*(U) transition modified by some *π*(U═N)→*f*(U) character, while the third band mainly originates from the *π*(U═N)→*f*(U) transition. The experimentally measured absorption bands for **2^{t}Bu** and **3Ph**[40,41] were well reproduced by our TDDFT calculations. Spin−orbit TD-B3LYP calculations of **2H** indicate that the spin−orbit coupling plays a significant role in the spectral study.

Finally, with the inclusion of solvation and spin−orbit coupling, free energies of formation reactions of *bis*-imido complexes were calculated. It is found that solvation is more important than spin−orbit coupling in calculations of reaction energies. The experimentally synthesized **2^{t}Bu**, **3Me**, and **3Ph** have been calculated to be thermodynamically favorable.[40,41]

■ ASSOCIATED CONTENT

Ⓢ Supporting Information

Tables of calculated bond orders and atomic charges (Tables S1 and S2); discussion of calculated charges; table of calculated energies of possible isomers of *cis*-**2Ph** and *cis*-**3Ph** (Table S3); tables of orbital compositions of **2H**, **2^{t}Bu**, **2Ph**, **3H**, **2UO$_2$**, and **3UO$_2$** (Tables S4 to S9); tables of absorptions of **2^{t}Bu**, **3H**, **3Ph**, and **3^{t}Bu′** (Tables S10 to S13); table of calculated

dx.doi.org/10.1021/ic401440w | Inorg. Chem. 2013, 52, 9143−9152

solvation and spin−orbit free energies (Table S14); table of thermodynamical energies of **3R** ⇌ **2R** + THF (Table S15). Figure of isomeric structures of *cis*-**2Ph** and *cis*-**3Ph** (Figure S1); figures of IR spectra of **2R**, **3R**, and **3^{t}Bu′** (S2 to S4); diagrams of orbital electron densities of **2H**, **2^{t}Bu**, **2Ph** (S5 to S7); energy-correlation diagram of **2H** at the C_1 and C_s symmetry (S8); figure of theoretically simulated absorption spectra of **2^{t}Bu** at different functionals (S9); plot of free energy ($\Delta_r G(\mathrm{sol+so})_{\mathrm{PBE}}$) of formation reaction (S10). This material is available free of charge via the Internet at http://pubs.acs.org.

AUTHOR INFORMATION

Corresponding Author

*E-mail: panqjitc@163.com.

Notes

The authors declare no competing financial interest.

ACKNOWLEDGMENTS

Q.-J.P. is grateful to Dr. Dimitri Laikov for providing the Priroda code. This work is supported by Fundamental Research Funds for the Central Universities (DL11CB07), National Natural Science Foundation of China (21273063, 30901136), Program for New Century Excellent Talents in University (NCET-11-0958), and Key Project of Chinese Ministry of Education (211048). Foundations for the Returned Overseas Chinese Scholars of Heilongjiang Province (LC2011C22) and State Education Ministry are greatly acknowledged. G.S. acknowledges funding from the Natural Sciences and Engineering Research Council of Canada (NSERC).

REFERENCES

(1) Hashke, J. M.; Stakebake, J. L. Handling, storage, and disposition of plutonium and uranium. In *The chemistry of the actinide and transactinide elements*; Morss, L. R., Edelstein, N. M., Fuger, J., Eds.; Springer: New York, 2006; pp 3199−3272.

(2) Rambo, B. M.; Sessler, J. L. *Chem.—Eur. J.* **2011**, *17*, 4946−4959.

(3) Choppin, G. R. *J. Radioanal. Nucl. Chem.* **2007**, *273*, 695−703.

(4) Choppin, G. R.; Jensen, M. P. Actinides in solution: complexation and kinetics. In *The chemistry of the actinide and transactinide elements*; Morss, L. R., Edelstein, N. M., Fuger, J., Eds.; Springer: New York, 2006; p 2554.

(5) Streit, M.; Ingold, F. *J. Eur. Ceram. Soc.* **2005**, *25*, 2687−2692.

(6) Thomas, S. H.; Padilla-Crespo, E.; Jardine, P. M.; Sanford, R. A.; Loffler, F. E. *Appl. Environ. Microbiol.* **2009**, *75*, 3679−3687.

(7) Clark, D. L.; Hobart, D. E.; Neu, M. P. *Chem. Rev.* **1995**, *95*, 25−48.

(8) Mathews, T.; Beaugelin-Seiller, K.; Garnier-Laplace, J.; Gilbin, R.; Adam, C.; Della-Vedova, C. *Environ. Sci. Technol.* **2009**, *43*, 6684−6690.

(9) Kim, Y. J.; Moon, J. W.; Roh, Y.; Brooks, S. C. *Environ. Geol.* **2009**, *58*, 1301−1307.

(10) Denning, R. G. *J. Phys. Chem. A* **2007**, *111*, 4125−4143.

(11) Bart, S. C.; Meyer, K., Highlights in uranium coordination chemistry. In *Organometallic and Coordination Chemistry of the Actinides*; Springer-Verlag: Berlin, Germany, 2008; Vol. *127*, pp 119−176.

(12) Alexander, V. *Chem. Rev.* **1995**, *95*, 273−342.

(13) Berthet, J. C.; Lance, M.; Nierlich, M.; Ephritikhine, M. *Eur. J. Inorg. Chem.* **2000**, 1969−1973.

(14) Berthet, J. C.; Nierlich, M.; Ephritikhine, M. *Chem. Commun.* **2003**, 1660−1661.

(15) Berthet, J. C.; Nierlich, M.; Ephritikhine, M. *Chem. Commun.* **2004**, 870−871.

(16) Berthet, J. C.; Nierlich, M.; Ephritikhine, M. *Angew. Chem., Int. Ed.* **2003**, *42*, 1952−1954.

(17) Oldham, W. J.; Oldham, S. M.; Scott, B. L.; Abney, K. D.; Smith, W. H.; Costa, D. A. *Chem. Commun.* **2001**, 1348−1349.

(18) Vaughn, A. E.; Barnes, C. L.; Duval, P. B. *J. Chem. Crystallogr.* **2007**, *37*, 779−782.

(19) Wilkerson, M. P.; Burns, C. J.; Paine, R. T.; Scott, B. L. *Inorg. Chem.* **1999**, *38*, 4156−4158.

(20) Alcock, N. W.; Flanders, D. J.; Brown, D. *J. Chem. Soc., Dalton Trans.* **1985**, 1001−1007.

(21) Fortier, S.; Hayton, T. W. *Coord. Chem. Rev.* **2010**, *254*, 197−214.

(22) Hayton, T. W. *Dalton Trans.* **2010**, *39*, 1145−1158.

(23) Brown, J. L.; Wu, G.; Hayton, T. W. *J. Am. Chem. Soc.* **2010**, *132*, 7248−7249.

(24) Boncella, J. M. *Nature* **2008**, *451*, 250−252.

(25) Sullivan, J. C.; Zielen, A. J.; Hindman, J. C. *J. Am. Chem. Soc.* **1961**, *83*, 3373−3378.

(26) Natrajan, L.; Burdet, F.; Pecaut, J.; Mazzanti, M. *J. Am. Chem. Soc.* **2006**, *128*, 7152−7153.

(27) Nocton, G.; Horeglad, P.; Pecaut, J.; Mazzanti, M. *J. Am. Chem. Soc.* **2008**, *130*, 16633−16645.

(28) Sullens, T. A.; Jensen, R. A.; Shvareva, T. Y.; Albrecht-Schmitt, T. E. *J. Am. Chem. Soc.* **2004**, *126*, 2676−2677.

(29) Arnold, P. L.; Jones, G. M.; Odoh, S. O.; Schreckenbach, G.; Magnani, N.; Love, J. B. *Nat. Chem.* **2012**, *4*, 221−227.

(30) Arnold, P. L.; Hollis, E.; White, F. J.; Magnani, N.; Caciuffo, R.; Love, J. B. *Angew. Chem., Int. Ed.* **2011**, *50*, 887−890.

(31) Arnold, P. L.; Patel, D.; Wilson, C.; Love, J. B. *Nature* **2008**, *451*, 315−318.

(32) Arney, D. S. J.; Burns, C. J.; Smith, D. C. *J. Am. Chem. Soc.* **1992**, *114*, 10068−10069.

(33) Arney, D. S. J.; Burns, C. J. *J. Am. Chem. Soc.* **1993**, *115*, 9840−9841.

(34) Arney, D. S. J.; Burns, C. J. *J. Am. Chem. Soc.* **1995**, *117*, 9448−9460.

(35) Warner, B. P.; Scott, B. L.; Burns, C. J. *Angew. Chem.* **1998**, *110*, 1005−1007.

(36) Arney, D. S. J.; Schnabel, R. C.; Scott, B. C.; Burns, C. J. *J. Am. Chem. Soc.* **1996**, *118*, 6780−6781.

(37) Brown, D. R.; Denning, R. G.; Jones, R. H. *J. Chem. Soc., Chem. Commun.* **1994**, 2601−2602.

(38) Brown, D. R.; Denning, R. G. *Inorg. Chem.* **1996**, *35*, 6158−6163.

(39) Williams, V. C.; Müller, M.; Leech, M. A.; Denning, R. G.; Green, M. L. H. *Inorg. Chem.* **2000**, *39*, 2538−2541.

(40) Hayton, T. W.; Boncella, J. M.; Scott, B. L.; Palmer, P. D.; Batista, E. R.; Hay, P. J. *Science* **2005**, *310*, 1941−1943.

(41) Hayton, T. W.; Boncella, J. M.; Scott, B. L.; Batista, E. R.; Hay, P. J. *J. Am. Chem. Soc.* **2006**, *128*, 10549−10559.

(42) Hayton, T. W.; Boncella, J. M.; Scott, B. L.; Batista, E. R. *J. Am. Chem. Soc.* **2006**, *128*, 12622−12623.

(43) Spencer, L. P.; Yang, P.; Scott, B. L.; Batista, E. R.; Boncella, J. M. *J. Am. Chem. Soc.* **2008**, *130*, 2930−2931.

(44) Spencer, L. P.; Gdula, R. L.; Hayton, T. W.; Scott, B. L.; Boncella, J. M. *Chem. Commun.* **2008**, 4986−4988.

(45) Spencer, L. P.; Schelter, E. J.; Yang, P.; Gdula, R. L.; Scott, B. L.; Thompson, J. D.; Kiplinger, J. L.; Batista, E. R.; Boncella, J. M. *Angew. Chem., Int. Ed.* **2009**, *48*, 3795−3798.

(46) Spencer, L. P.; Yang, P.; Scott, B. L.; Batista, E. R.; Boncella, J. M. *Inorg. Chem.* **2009**, *48*, 11615−11623.

(47) Spencer, L. P.; Yang, P.; Scott, B. L.; Batista, E. R.; Boncella, J. M. *Inorg. Chem.* **2009**, *48*, 2693−2700.

(48) Spencer, L. P.; Yang, P.; Scott, B. L.; Batista, E. R.; Boncella, J. M. *C. R. Chim.* **2010**, *13*, 758−766.

(49) Spencer, L. P.; Yang, P.; Minasian, S. G.; Jilek, R. E.; Batista, E. R.; Boland, K. S.; Boncella, J. M.; Conradson, S. D.; Clark, D. L.; Hayton, T. W.; Kozimor, S. A.; Martin, R. L.; MacInnes, M. M.; Olson, A. C.; Scott, B. L.; Shuh, D. K.; Wilkerson, M. P. *J. Am. Chem. Soc.* **2013**, *135*, 2279−2290.

(50) Cramer, R. E.; Maynard, R. B.; Paw, J. C.; Gilje, J. W. *J. Am. Chem. Soc.* **1981**, *103*, 3589−3590.
(51) Cramer, R. E.; Maynard, R. B.; Paw, J. C.; Gilje, J. W. *Organometallics* **1983**, *2*, 1336−1340.
(52) Stevens, R. C.; Bau, R.; Cramer, R. E.; Afzal, D.; Gilje, J. W.; Koetzle, T. F. *Organometallics* **1990**, *9*, 694−697.
(53) Villiers, C.; Ephritikhine, M. *Chem.—Eur. J.* **2001**, *7*, 3043−3051.
(54) Cantat, T.; Arliguie, T. r. s.; Noël, A.; Thuéry, P.; Ephritikhine, M.; Floch, P. L.; Mézailles, N. *J. Am. Chem. Soc.* **2009**, *131*, 963−972.
(55) Lyon, J. T.; Andrews, L.; Hu, H.-S.; Li, J. *Inorg. Chem.* **2008**, *47*, 1435−1442.
(56) Ma, G.; Ferguson, M. J.; McDonald, R.; Cavell, R. G. *Inorg. Chem.* **2011**, *50* (14), 6500−6508.
(57) Brennan, J. G.; Andersen, R. A. *J. Am. Chem. Soc.* **1985**, *107*, 514−516.
(58) Villiers, C.; Thuery, P.; Ephritikhine, M. *Angew. Chem., Int. Ed.* **2008**, *47*, 5892−5893.
(59) Schreckenbach, G.; Shamov, G. A. *Acc. Chem. Res.* **2010**, *43*, 19−29.
(60) Kaltsoyannis, N. *Chem. Soc. Rev.* **2003**, *32*, 9−16.
(61) Kaltsoyannis, N. *Inorg. Chem.* **2000**, *39*, 6009−6017.
(62) Kaltsoyannis, N.; Scott, P. *The f elements*; Oxford University Press: Oxford, U.K., 1999.
(63) Gagliardi, L.; Roos, B. O. *Nature* **2005**, *433*, 848−851.
(64) Pan, Q.-J.; Odoh, S. O.; Schreckenbach, G.; Arnold, P. L.; Love, J. B. *Dalton Trans.* **2012**, *41*, 8878−8885.
(65) Pan, Q.-J.; Schreckenbach, G.; Arnold, P. L.; Love, J. B. *Chem. Commun.* **2011**, *47*, 5720−5722.
(66) Pan, Q. J.; Shamov, G. A.; Schreckenbach, G. *Chem.—Eur. J.* **2010**, *16*, 2282−2290.
(67) Pan, Q. J.; Schreckenbach, G. *Inorg. Chem.* **2010**, *49*, 6509−6517.
(68) Laikov, D. N. *Chem. Phys. Lett.* **1997**, *281*, 151−156.
(69) Laikov, D. N., Ph.D. Thesis, Moscow State University, Moscow, Russia, 2000.
(70) Laikov, D. N. *Chem. Phys. Lett.* **2005**, *416*, 116−120.
(71) Laikov, D. N.; Ustynyuk, Y. A. *Russ. Chem. Bull.* **2005**, *54*, 820−826.
(72) Laikov, D. N. *J. Comput. Chem.* **2007**, *28*, 698−702.
(73) Mayer, I. *Simple theorems, proof and derivations in quantum chemistry*; Kluwer Academic /Plenum Publishers: New York, 2003.
(74) Perdew, J. P.; Burke, K.; Ernzerhof, M. *Phys. Rev. Lett.* **1996**, *77*, 3865−3868.
(75) Laikov, D. N. *An Implementation of the Scalar Relativistic Density Functional Theory for Molecular Calculatios with Gaussian Basis Sets*; DFT2000 Conference: Menton, France, 2000.
(76) Dyall, K. G. *J. Chem. Phys.* **1994**, *100*, 2118−2127.
(77) Shamov, G. A.; Schreckenbach, G. *J. Am. Chem. Soc.* **2008**, *130*, 13735−13744.
(78) te Velde, G.; Bickelhaupt, F. M.; Baerends, E. J.; Fonseca Guerra, C.; Van Gisbergen, S. J. A.; Snijders, J. G.; Ziegler, T. *J. Comput. Chem.* **2001**, *22*, 931−967.
(79) Fonseca Guerra, C.; Snijders, J. G.; te Velde, G.; Baerends, E. J. *Theor. Chem. Acc.* **1998**, *99*, 391−403.
(80) Baerends, E. J.; Ziegler, T.; Autschbach, J.; Bashford, D.; Bérces, A.; Bickelhaupt, F. M.; Bo, C.; Boerrigter, P. M.; Cavallo, L.; Chong, D. P.; Deng, L.; Dickson, R. M.; Ellis, D. E.; van Faassen, M.; Fan, L.; Fischer, T. H.; Fonseca Guerra, C.; Ghysels, A.; Giammona, A.; van Gisbergen, S. J. A.; Götz, A. W.; Groeneveld, J. A.; Gritsenko, O. V.; Grüning, M.; Gusarov, S.; Harris, F. E.; van den Hoek, P.; Jacob, C. R.; Jacobsen, H.; Jensen, L.; Kaminski, J. W.; van Kessel, G.; Kootstra, F.; Kovalenko, A.; Krykunov, M. V.; van Lenthe, E.; McCormack, D. A.; Michalak, A.; Mitoraj, M.; Neugebauer, J.; Nicu, V. P.; Noodleman, L.; Osinga, V. P.; Patchkovskii, S.; Philipsen, P. H. T.; Post, D.; Pye, C. C.; Ravenek, W.; Rodríguez, J. I.; Ros, P.; Schipper, P. R. T.; Schreckenbach, G.; Seldenthuis, J. S.; Seth, M.; Snijders, J. G.; Solà, M.; Swart, M.; Swerhone, D.; te Velde, G.; Vernooijs, P.; Versluis, L.; Visscher, L.; Visser, O.; Wang, F.; Wesolowski, T. A.; van Wezenbeek, E. M.; Wiesenekker, G.; Wolff, S. K.; Woo, T. K.; Yakovlev, A. L. *ADF, ADF2010.02*; SCM, Theoretical Chemistry, Vrije Universiteit: Amsterdam, The Netherlands, 2010.
(81) Pye, C. C.; Ziegler, T. *Theor. Chem. Acc.* **1999**, *101*, 396−408.
(82) Klamt, A.; Jonas, V.; Burger, T.; Lohrenz, J. C. W. *J. Phys. Chem. A* **1998**, *102*, 5074−5085.
(83) Shamov, G. A.; Schreckenbach, G. *J. Phys. Chem. A* **2006**, *110*, 9486−9499.
(84) van Lenthe, E.; Ehlers, A.; Baerends, E. J. *J. Chem. Phys.* **1999**, *110*, 8943−8953.
(85) van Lenthe, E.; Baerends, E. J.; Snijders, J. G. *J. Chem. Phys.* **1994**, *101*, 9783−9792.
(86) van Lenthe, E.; Baerends, E. J.; Snijders, J. G. *J. Chem. Phys.* **1993**, *99*, 4597−4610.
(87) van Lenthe, E.; Snijders, J.; Baerends, E. *J. Chem. Phys.* **1996**, *105*, 6505−6516.
(88) Becke, A. D. *Phys. Rev. A* **1988**, *38*, 3098−3100.
(89) Lee, C. T.; Yang, W. T.; Parr, R. G. *Phys. Rev. B* **1988**, *37*, 785−789.
(90) Becke, A. D. *J. Chem. Phys.* **1993**, *98*, 5648−5652.
(91) Stephens, P. J.; Devlin, F. J.; Chabalowski, C. F.; Frisch, M. J. *J. Phys. Chem.* **1994**, *98*, 11623−11627.
(92) Ernzerhof, M.; Scuseria, G. E. *J. Chem. Phys.* **1999**, *110*, 5029−5036.
(93) Grimme, S. *J. Comput. Chem.* **2004**, *25*, 1463−1473.
(94) Schreckenbach, G.; Hay, P. J.; Martin, R. L. *Inorg. Chem.* **1998**, *37*, 4442−4451.
(95) Wang, X.; Andrews, L.; Vlaisavljevich, B.; Gagliardi, L. *Inorg. Chem.* **2011**, *50* (8), 3826−3831.
(96) Réal, F.; Gomes, A. S. P.; Visscher, L.; Vallet, V. r.; Eliav, E. *J. Phys. Chem. A* **2009**, *113*, 12504−12511.
(97) Tecmer, P.; Gomes, A. S. P.; Ekström, U.; Visscher, L. *Phys. Chem. Chem. Phys.* **2011**, *13*, 6249−6259.
(98) Gagliardi, L.; Grenthe, I.; Roos, B. O. *Inorg. Chem.* **2001**, *40*, 2976−2978.
(99) Dognon, J. P.; Clavaguéra, C.; Pyykkö, P. *J. Am. Chem. Soc.* **2008**, *131*, 238−243.
(100) Pierloot, K.; van Besien, E.; van Lenthe, E.; Baerends, E. J. *J. Chem. Phys.* **2007**, *126*, 194311.